Applied Surface Science 336 (2015) 73–78

Contents lists available at ScienceDirect

Applied Surface Science

journal homepage: www.elsevier.com/locate/apsusc

Laser annealing of plasma-damaged silicon surface

T. Sameshima [a,*], M. Hasumi [a], T. Mizuno [b]

[a] Tokyo University of Agriculture and Technology, Tokyo, 184-8588, Japan
[b] Kanagawa University, Kanagawa, 259-1293, Japan

ARTICLE INFO

Article history:
Received 24 May 2014
Received in revised form 16 August 2014
Accepted 22 September 2014
Available online 18 October 2014

Keywords:
Minority carrier effective lifetime
Plasma irradiation
Laser irradiation
Interface traps
Hysteresis
Microwave absorption
Carrier recombination

ABSTRACT

13.56 MHz capacitance coupled Ar plasma irradiation at 50 W for 120 s caused serious damage at SiO_2/Si interfaces for n-type 500-μm-thick silicon substrates. The 635-nm-light induced minority carrier effective lifetime (τ_{eff}) was decreased from 1.7×10^{-3} (initial) to 1.0×10^{-5} s by Ar plasma irradiation. Moreover, the capacitance response at 1 MHz alternative voltage as a function of the bias voltage (*C*–*V*) was changed to hysteresis characteristic associated with the density of charge injection type interface traps at the mid gap (D_{it}) at 9.1×10^{11} cm^{-2} eV^{-1}. Subsequent 940-nm laser annealing at 3.7×10^{4} W/cm^2 for 4.0×10^{-3} s markedly increased τ_{eff} to 1.7×10^{-3} s and decreased D_{it} to 2.1×10^{10} cm^{-2} eV^{-1}. The hysteresis phenomenon was reduced in *C*–*V* characteristics. Laser annealing effectively decreased the density of plasma induced carrier recombination and trap states. However, laser annealing with a high power intensity of 4.0×10^{4} W/cm^2 seriously caused a thermal damage associated with a low τ_{eff} and a high D_{it} with no hysteresis characteristic.

© 2014 Elsevier B.V. All rights reserved.

1. Introduction

Laser annealing has been widely used for modification of semiconductor surfaces. High power pulsed or continuous wave (CW) laser rapidly heats the surface regions to a high temperature or melts them above melting temperatures. After the termination of laser light, the surface regions rapidly cooled down. No substrate heating is necessary because laser irradiation energy effectively concentrates in the surface region during short irradiation time [1–7]. Laser induced crystallization method has been developed and it has been applied for fabricating poly-crystalline silicon thin film transistor for flat panel display devices [8–26]. Laser annealing also makes it possible to activate semiconductor implanted with dopant atoms and diffuse dopant atoms into semiconductor which is so-called laser doping [27–29]. Laser induced activation is attractive to form shallow PN junction because of no marked impurity diffusion during short heating duration. Laser doping has been also paid attention for fabricating pn junction for solar cells [30–36].

Laser annealing is also attractive for reduction of the density of interface traps at the semiconductor surface regions. Reduction of the density of interface traps by laser annealing at low processing temperature and in short tact time will be practical for semiconductor device processing. Especially for photo devices such as solar cells and high sensitivity photo sensors, a low annihilation rate of photo induced carriers is required. A simple surface passivation method will be important for photo device fabrication.

In this paper, we report laser annealing of silicon surface using 940-nm continuous wave (CW) semiconductor laser. Ar plasma irradiation is applied to the SiO_2/Si interface region. It causes a high density of interface traps at SiO_2/Si interface region and decreased the effective minority carrier lifetime (τ_{eff}), which is an important parameter for evaluating the photoconductive properties of semiconductors [37–45]. It also causes a marked hysteresis property in capacitance response with bias voltage (*C*–*V*). We experimentally demonstrate that laser annealing effectively decreases the density of interface traps; τ_{eff} is increased to a similar value of the initial silicon sample and the hysteresis property in *C*–*V* characteristics is cured. We also show that the laser power has an upper limit for laser annealing. Different type of defect states is generated by laser annealing with a high power intensity.

2. Experimental

15 Ωcm n-type 500-μm-thick Czochralski grown single crystalline silicon substrates with an orientation of (1 0 0) were prepared. Phosphorus atoms with a concentration of 2.9×10^{14} cm^{-3} were doped. Other impurities such as heavy metals were not detected within the analysis limit of 10^{7} cm^{-3}. The top and rear surfaces were coated with 100-nm-thick thermally grown SiO_2 layers formed in 1100 °C wet oxygen atmosphere. The silicon samples

* Corresponding author. Tel.: +81 42 388 7109; fax: +81 42 388 7109.
E-mail address: tsamesim@cc.tuat.ac.jp (T. Sameshima).

http://dx.doi.org/10.1016/j.apsusc.2014.09.142
0169-4332/© 2014 Elsevier B.V. All rights reserved.

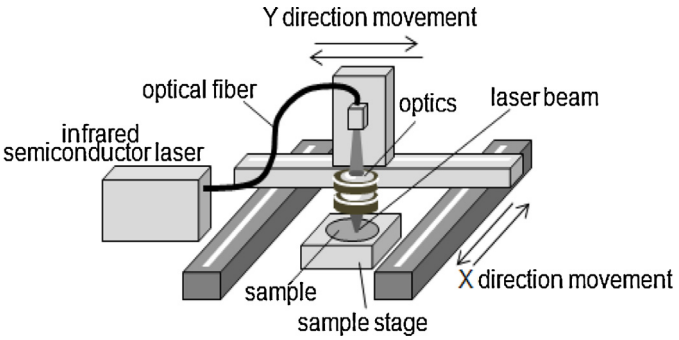

Fig. 1. Schematic apparatus of laser irradiation.

were heated with 940-nm infrared CW semiconductor laser for laser annealing (annealing laser) [46]. Fig. 1 shows a schematic apparatus of laser annealing. The laser beam with a maximum power of 25 W was introduced using an optical fiber. The optical fiber and optics with a lens were mounted on an *X*–*Y* mobile stage. The laser beam was focused by the lens to a spot with a Gaussian intensity distribution and a diameter of 200 μm at full width at maximum half at the sample surface. Samples were placed on a 1-mm-thick quartz glass plate in a normal direction to the laser beam. The laser beam was moved in the Y-direction at 5 cm/s at power intensities ranging from 2.7×10^4 to 4.4×10^4 W/cm^2 at sample surface. The irradiation duration was 4.0×10^{-3} s. The laser beam was stepwise moved in the X-direction at a step of 100 μm. The top surface of the sample was entirely heated by laser irradiation with an overlapping ratio of 50% for 4.0×10^{-3} s.

The top surfaces of the samples were irradiated by 13.56 MHz radio-frequency (RF)-capacitance-coupled Ar plasma at 50 W and 1.0 Pa for 120 s [47]. A sample was placed on a metal plate electrically grounded in a chamber facing a metal electrode applied at RF voltage. Ar gas was introduced at 50 sccm under evacuation using a turbo-molecular pump, as shown in Fig. 2.

To measure τ_{eff} precisely, we used a 9.35-GHz-microwave-transmittance measurement system, as shown in Fig. 3 [48–50]. The system had waveguide tubes, which had a narrow gap where a sample was placed to measure τ_{eff}. CW 635 and 980 nm laser diode (illumination laser) lights were introduced to the waveguide tubes. The light intensities were set at 1.5 and 0.98 mW/cm^2 on the sample surface for 635 and 980 nm illumination laser lights, respectively, to realize the same photon flux between the two different wavelength lights. The microwave transmissivities of the sample

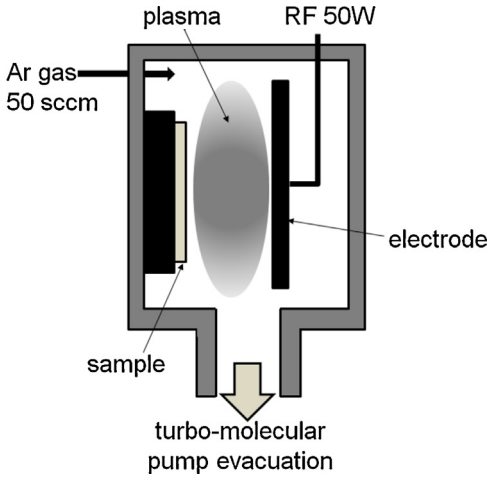

Fig. 2. Schematic of apparatus for 13.56 MHz radio-frequency Ar plasma irradiation at 50 W and at room temperature.

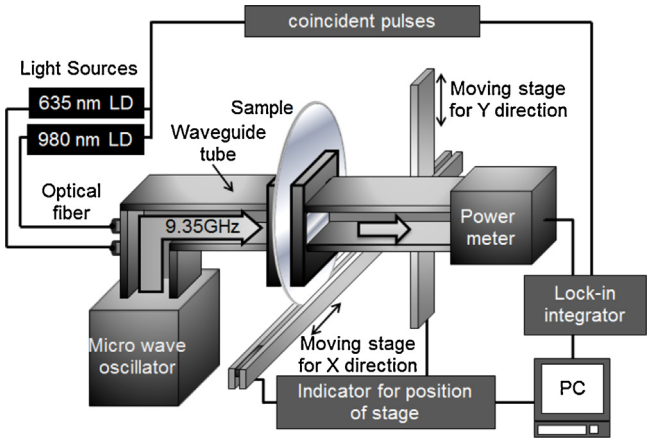

Fig. 3. Schematic of apparatus for a 9.35 GHz microwave transmittance measurement system for measuring τ_{eff} of sample wafers with 635 and 980 nm light illuminations.

in the dark (T_d), and under light illumination (T_p), were measured for duration of 4 s each [48]. The logarithmic ratio of $\ln(T_d/T_p)$ is proportional to the density of minority carriers per unit area (N). Because N is given by τ_{eff} and the carrier generation rate G per unit area as [48,49],

$$N = t_{eff} \times G, \quad (1)$$

τ_{eff} is determined by $\ln(T_d/T_p)$. The uncertainty coefficients between $\ln(T_d/T_p)$ and N were determined by the method of microwave absorption under multiply periodic pulsed light illumination [49], which gave τ_{eff} independently of the effective loss of the optical reflectivity, which depends on the incident angle of light and the surface structure in general, although the measurement accuracy of τ_{eff} for multiply periodic pulsed light illumination method is 2×10^{-5} s. The detection limit of τ_{eff} in the present CW light illumination system was 5×10^{-7} s. τ_{eff} in the case of light illumination to the top surface, τ_{eff} (top), and in the case of light illumination to the rear surface, τ_{eff} (rear) were measured. The penetration depth (d) for 635 nm light was about 3 μm, while that for 980 nm light was 125 μm [51].

After the microwave transmittance measurement, we prepared MOS type samples for measuring *C*–*V* characteristics [52]. In advance of metal electrodes, the top surfaces of SiO_2/Si of the samples were irradiated with Ar plasma and subsequently annealed with the annealing laser at 3.7×10^4 W/cm^2. The SiO_2/Si interface was also annealed with the annealing laser at 4.4×10^4 W/cm^2 and subsequently annealed with the annealing laser at 3.7×10^4 W/cm^2. The SiO_2 layers at the rear surface were removed by 5% hydrofluoric acid. To form MOS samples, Al metal electrodes with an area of 0.1 cm × 0.1 cm were formed at the top surface by the vacuum evaporation. Al metal electrode was also formed entirely on the rear surface. The *C*–*V* characteristics at 1 MHz alternative voltage with an amplitude of 10 mV were measured in the dark field as shown in Fig. 4. The bias voltage was applied stepwise with 0.1 V from +15 to −15 V and then −15 to +15 V. Each bias voltage was maintained for 4 s in order to realize measurement in the electrically steady state. Five MOS samples were measured for each conditions. *C*–*V* characteristics were obtained by those average values. The accuracy of the *C*–*V* measurement was 1×10^{-9} F/cm^2.

3. Results

To analyze experimental τ_{eff}, we developed a homemade finite-element numerical calculation program including theories of carrier generation associated with optical absorption coefficients,

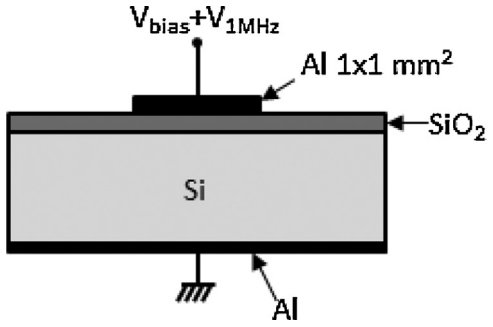

Fig. 4. Schematic of cross section of MOS sample and voltage application for *C–V* measurements.

carrier diffusion, and annihilation for estimating the surface recombination velocity on the top surface (S_{top}) and rear surface (S_{rear}) and the bulk lifetime τ_b [53]. The photo induced minority carriers diffuse into the substrate, when CW laser light (illumination laser) is illuminated as [48,50,53,54]

$$D\frac{\partial^2 n(x)}{\partial x^2} + \frac{n(x)}{\tau_b} - g(x) = 0, \quad (2)$$

where $n(x)$, $g(x)$, and D are the carrier volume density, the carrier generation rate at a depth of x, and the diffusion constant of minority carriers, respectively. Carrier generation occurs in the substrate bulk, which depends on the optical absorption coefficient at a certain light wavelength. Carrier annihilation occurs with τ_b. When the top surface was illuminated with light, the boundary conditions of carrier generation and carrier recombination ratios are given as

$$D\left.\frac{\partial n(x)}{\partial x}\right|_{x=0} = S_{top}n(0) - g(0)\Delta x, \quad (3a)$$

$$D\left.\frac{\partial n(x)}{\partial x}\right|_{x=L} = -S_{rear}n(L) - g(L)\Delta x, \quad (3b)$$

where L is the thickness of the semiconductor substrate, and Δx is the unit lattice length of the present calculation. In the case of rear surface illumination, S_{top} and S_{rear} exchanged each other in Eqs. (3a) and (3b). G determined by the method of microwave absorption under multiply periodic pulsed light illumination [49] gives the carrier generation rate $g(x)$ per unit volume using d [51] as

$$g(x) = \frac{G}{d}e^{-x/d}, \quad (4)$$

The most possible S_{top} and S_{rear} were determined by the best coincidence between the experimental and calculated τ_{eff} values.

Fig. 5 shows τ_{eff} (top) (open circles) and τ_{eff} (rear) (solid circles) as a function of laser power intensity for Ar plasma irradiated samples in the illumination cases of the 635 (a) and 980 nm illumination lasers (b). For the initial sample τ_{eff} (top) and τ_{eff} (rear) had a high value of 1.5×10^{-3} s. When Ar plasma was irradiated to the initial sample, τ_{eff} (top) and τ_{eff} (rear) decreased to 1.0×10^{-5} and 1.0×10^{-4} s in the illumination case of the 635 nm illumination laser, as shown by arrows in Fig. 5(a). They also decreased to 5.5×10^{-5} and 1.0×10^{-4} s, in the illumination case of 980 nm illumination laser, as shown by arrows in Fig. 5(b). The plasma irradiated sample was heated by the annealing laser with stepwise increasing its power intensity. τ_{eff} (top) and τ_{eff} (rear) markedly increased to about 1.7×10^{-3} s, almost the same as that of the initial sample, as the annealing laser power intensity increased from 2.7×10^4 up to 3.6×10^4 W/cm^2 in the illumination cases of the 635 and 980 nm illumination lasers. The laser annealing cured the defect states caused by the Ar plasma irradiation. However, τ_{eff} (top) and τ_{eff} (rear) were decreased again by laser annealing above 4.0×10^4 W/cm^2. τ_{eff} (top) decreased to 2.2×10^{-5} and

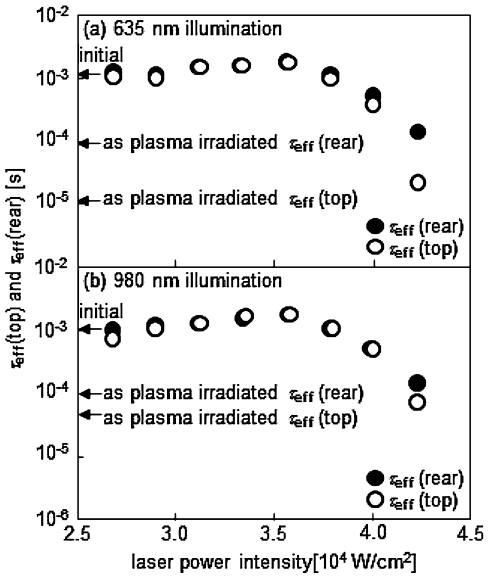

Fig. 5. τ_{eff} (top) (open circles) and τ_{eff} (rear) (solid circles) as a function of laser power intensity for Ar plasma irradiated samples in the cases of 635 (a) and 980 nm illuminations (b). For the initial sample τ_{eff} (top) and τ_{eff} (rear) had a high value of 1.5×10^{-3} s. Arrows show τ_{eff} (top) and τ_{eff} (rear) for initial and Ar plasma irradiated samples.

7.6×10^{-5} s at 4.25×10^4 W/cm^2 in the illumination cases of the 635 and 980 nm illumination lasers. Heat flow calculation using a homemade numerical finite element program [29] estimated temperature increase to 1070 K at the top surface under the conditions of a laser intensity of 4.25×10^4 W/cm^2 and a light reflection loss of 17% at 940 nm. The calculation suggests that the silicon surface region was not melted by the irradiation condition given above.

Fig. 6 shows *C–V* characteristics for the initial sample (a), plasma irradiated sample (b), and then 3.7×10^4 W/cm^2 laser annealed sample (c), Sharp change in capacitance was observed

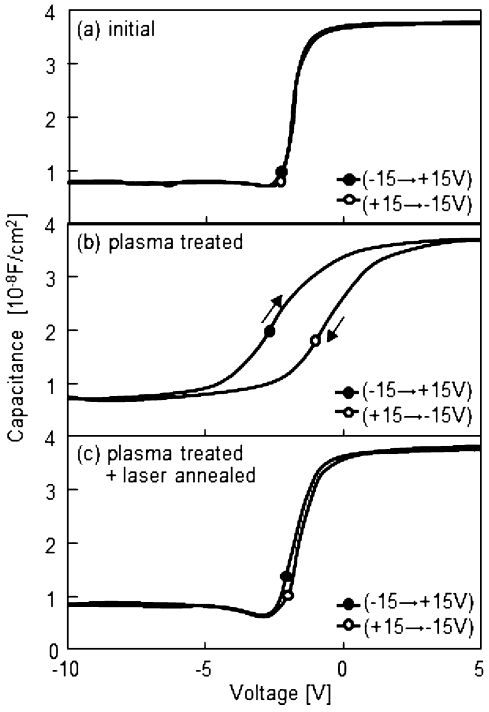

Fig. 6. Capacitance as a function of bias voltage for the initial sample (a), plasma irradiated sample (b), and then 3.7×10^4 W/cm^2 laser irradiated sample (c).

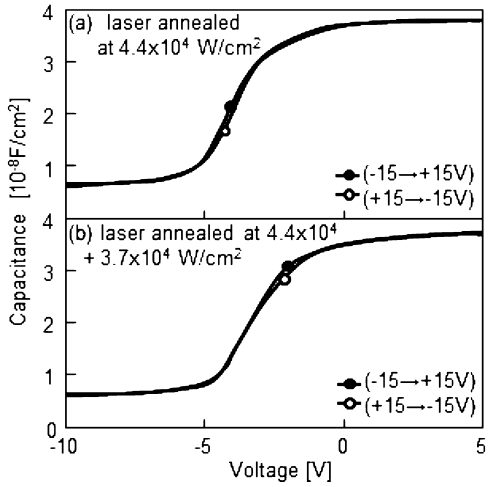

Fig. 7. Capacitance as a function of bias voltage for 4.4×10^4 W/cm^2 laser irradiated sample (a) and subsequently 3.7×10^4 W/cm^2 laser irradiated sample (b).

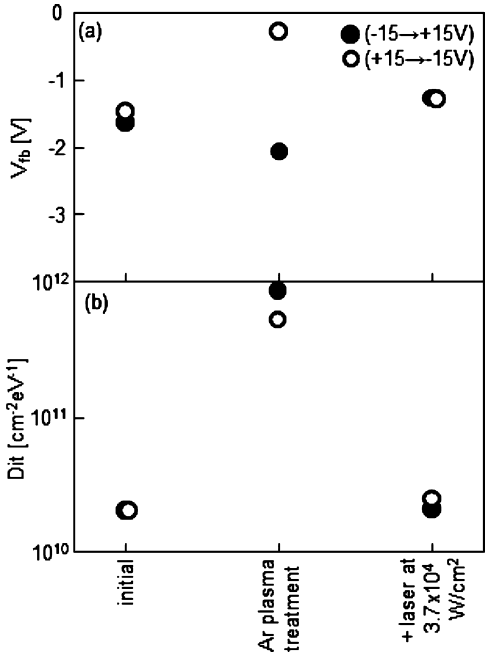

Fig. 8. V_{fb} (a) and D_{it} (b) in the cases of initial, Ar plasma, and subsequent 3.7×10^4 W/cm^2 laser irradiations.

for the initial sample. It means that the sample had a low density of interface traps. On the other hand, Ar plasma treatment made capacitance change very gradual and caused a serious hysteresis characteristic, as shown in Fig. 6(b). The subsequent laser annealing at 3.7×10^4 W/cm^2 made capacitance change sharp and reduced hysteresis characteristic like initial one, as shown in Fig. 6(a) and (c).

The laser annealing at 4.4×10^4 W/cm^2 also made change in capacitance gradual because of generation of interface trap states, as shown in Fig. 7(a). No hysteresis characteristic was observed. Subsequent laser annealing at 3.7×10^4 W/cm^2 hardly made change in capacitance in contrast to Ar plasma irradiation case, as shown in Fig. 7(b).

4. Discussion

High values of τ_{eff} (top) and τ_{eff} (rear) shown by arrows in Fig. 5 means that the initial sample had a high quality crystalline bulk and the surfaces well passivated with thermally grown SiO_2 layers. On the other hand, Ar plasma irradiation decreased τ_{eff} (top) and τ_{eff} (rear) to 1.0×10^{-5} and 1.0×10^{-4} s, in the illumination case of the 635 nm illumination laser, and to 5.5×10^{-5} and 1.0×10^{-4} in the illumination case of the 980 nm illumination laser shown by arrows in Fig. 5. Those results show that the plasma irradiation caused a high density of defect states at the top surface. The numerical calculation resulted in that S_{top} was increased from 17 to 4500 cm/s by the plasma irradiation. The subsequent laser annealing markedly increased τ_{eff} (top) and τ_{eff} (rear) to about 1.7×10^{-3} s almost the same as that of the initial sample, for the power intensity of the annealing laser between 2.7×10^4 and 3.6×10^4 W/cm^2. However, laser annealing at a high power intensity caused thermal damage. τ_{eff} (top) and τ_{eff} (rear) were decreased by laser annealing above 4.0×10^4 W/cm^2. τ_{eff} (top) decreased to 2.2×10^{-5} and 7.6×10^{-5} s at 4.25×10^4 W/cm^2 in the illumination cases of the 635 and 980 nm illumination lasers. S_{top} was increased again 2300 cm/s by the laser annealing. Those results mean that a high density of carrier recombination defect sites was generated at the surface region by laser annealing with a high power intensity. The defect sites caused by laser annealing effectively annihilate photo-induced carriers generated by illuminations of the 635 and 980 nm illumination lasers to the top surface.

Gradual change in the *C–V* curves shown in Fig. 6(b) means that Ar plasma irradiation caused a substantial density of interface traps, while the *C–V* curves with sharp changes of the initial sample shown in Fig. 6(a) means a low density of interface traps. Moreover, Ar plasma irradiation caused a marked hysteresis characteristic shown in Fig. 6(b). In the hysteresis characteristic, the capacitance per unit area decreased at higher bias voltages in the downward application case from +15 to −15 V than that at higher bias voltages in the upward application case from −15 to +15 V. This suggests that negative charges were injected near the SiO_2/Si interface during bias voltages application from +15 to −15 V. Subsequent the laser annealing at 3.7×10^4 W/cm^2 made capacitance change sharp with no hysteresis. Defects were reduced by the laser annealing. On the other hand, the laser annealing at 4.4×10^4 W/cm^2 also caused substantial interface trap states. But no hysteresis characteristic was observed in *C–V* characteristics. This result indicates that trap states caused by the laser annealing locates deep energy levels whose occupied probability was determined by the surface Fermi level with absence of non-thermally equilibrium charge injection.

The *C–V* curves shown in Figs. 6 and 7 were analyzed. The capacitances of the SiO_2 layer and the depletion region per unit area was derived from the maximum and minimum capacitance of the *C–V* curves. The flat band voltage (V_{fb}) was obtained from the capacitances of the SiO_2 layer and Debye length of the n-type silicon substrate. The density of interface traps at the mid gap (D_{it}) were given by capacitance of interface traps for the Fermi level positioned at the mid gap at the interface obtained from slope of the *C–V* curves [52]. Fig. 8 shows V_{fb} (a) and D_{it} (b) in the cases of initial, Ar plasma, and the subsequent 3.7×10^4 W/cm^2 laser annealing. The initial sample had a V_{fb} value of −1.5 V. Ar plasma irradiation changed V_{fb} to −0.3 and −2.1 V in the cases of bias voltage applied downward from +15 to −15 V and upward from −15 to +15 V, respectively, associated with hysteresis *C–V* characteristics. Negative and positive charges were injected to the traps during bias voltage applications. The 3.7×10^4 W/cm^2 laser annealing markedly changed V_{fb} to −1.3 V, which was lower than the initial value. This indicates that the fixed oxide charge density was decreased by the laser annealing. The laser annealing reduced hysteresis *C–V* characteristic as well as reduced V_{fb} compared to the initial value. The initial sample had a low D_{it} of 2.0×10^{10} cm^{-2} eV^{-1} (measurement lower limit). Ar plasma irradiation increased D_{it} to 5.3×10^{11} and 9.1×10^{11} cm^{-2} eV^{-1} in the case of bias voltage applied downward from +15 to −15 V and upward from −15 to +15 V, respectively, as shown in Fig. 8(b). The 3.7×10^4 W/cm^2 laser

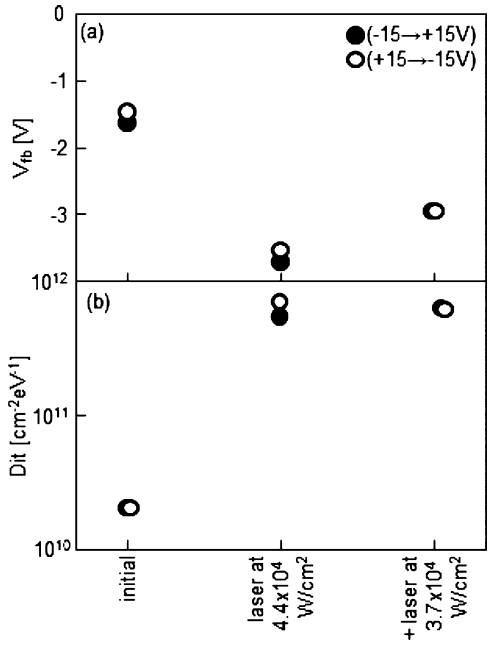

Fig. 9. V_{fb} (a) and D_{it} (b) in the cases of initial, 4.4×10^4, and subsequent 3.7×10^4 W/cm^2 laser irradiations.

annealing markedly decreased D_{it} to 2.3×10^{10} cm^{-2} eV^{-1}, which was almost same value of the initial sample.

Fig. 9 shows V_{fb} (a) and D_{it} (b) in the cases of initial, 4.4×10^4 W/cm^2 laser annealing, and subsequent the 3.7×10^4 W/cm^2 laser annealing. V_{fb} was decreased to −3.7 V by the 4.4×10^4 W/cm^2 laser annealing in the cases of the two bias voltage application modes. It was slightly increased to −3.0 V by subsequent the 3.7×10^4 W/cm^2 laser annealing, as shown in Fig. 9(a). The laser annealing at 4.4×10^4 W/cm^2 markedly increased D_{it} to 6.8×10^{11} cm^{-2} eV^{-1}, which was similar to D_{it} caused by Ar plasma irradiation. However, the subsequent 3.7×10^4 W/cm^2 laser annealing hardly decreased the value of D_{it} in contrast to the case of Ar plasma followed by the 3.7×10^4 W/cm^2 laser annealing.

Via those experimental results and analyses, we interpret that plasma irradiation caused substantial charge injection type defects at the SiO_2/Si interface region. High energy ultra violet light in plasma probably caused bond breaking of Si–Si or Si–O and made energy states in the band gap. That defect formation is serious problem because plasma processing has been widely used in semiconductor device fabrication. The present work revealed that the plasma induced defect states were easily eliminated by subsequent laser annealing. Laser rapid annealing is practical and will be applicable for high quality semiconductor device fabrication. However, laser-induced thermal damage by a high power intensity can cause different type of defects. *C–V* characteristics suggested that the defects were formed at deep energy levels in the band gap. We recently developed a similar technique of microwave annealing for reducing defects in silicon [50,55]. Plasma-induced defects were markedly reduced in solid state by irradiation of low intensity of microwave at 10 W/cm^2 at most. Although the samples are entirely heated by microwave annealing, there is no serious thermal damage associated with decrease in τ_{eff}. A combination of laser annealing and microwave annealing will be promising for effective defect reduction in semiconductors.

Summary

We investigated laser-induced passivation silicon surface using 940-nm semiconductor laser annealing. 15 Ωcm n-type 500-μm-thick silicon substrates coated with 100-nm-thick thermally grown SiO_2 layers were prepared. Ar plasma irradiation decreased τ_{eff} (top) and τ_{eff} (rear) to 1.0×10^{-5} and 1.0×10^{-4} s in the case of 635 nm illumination. It also decreased them to 5.5×10^{-5} and 1.0×10^{-4} s in the case of 980 nm illumination. The numerical calculation revealed that S_{top} was increased from 17 to 4500 cm/s by the plasma irradiation. The plasma induced defects were cured by laser annealing. τ_{eff} (top) and τ_{eff} (rear) markedly increased to 1.7×10^{-3} s for laser power intensity between 2.7×10^4 and 3.6×10^4 W/cm^2. *C–V* characteristics revealed that Ar plasma irradiation caused charge injection type interface defects ranging from 5.3×10^{11} to 9.1×10^{11} cm^{-2} eV^{-1}. 3.7×10^4 W/cm^2 laser annealing markedly decreased D_{it} to 2.3×10^{10} cm^{-2} eV^{-1}, which was almost same value of the initial sample. Moreover, the laser annealing at 4.4×10^4 W/cm^2 markedly increased D_{it} to 6.8×10^{11} cm^{-2} eV^{-1} similar to D_{it} caused by Ar plasma irradiation. No hysteresis *C–V* characteristic was observed. Subsequent 3.7×10^4 W/cm^2 laser annealing hardly decreased D_{it} in contrast to the case of Ar plasma followed by 3.7×10^4 W/cm^2 laser annealing. Those experimental results revealed that laser annealing cured the charge injection type defects caused by Ar plasma irradiation, and laser annealing with a high power intensity also can cause thermal damage with a high D_{it}.

Acknowledgements

This work was partly supported by Grant-in-Aid for Science Research C (no. 25420282) from the Ministry of Education, Culture, Sports, Science and Technology of Japan, and Sameken Co., Ltd., Japan.

References

[1] P.L. Liu, R. Yen, N. Bloembergen, R.T. Hodson, Appl. Phys. Lett. 34 (1979) 864.
[2] R. Tsu, R.T. Hodgson, T.Y. Tan, J.E. Baglin, Phys. Rev. Lett. 42 (1979) 1356.
[3] D.H. Lowndes, G.H. Kirkpatrick Jr., S.J. Pennycook, S.P. Withrow, D.N. Mashburn, Appl. Phys. Lett. 48 (1986) 1389.
[4] R.F. Wood, C.E. Giles, Rhys. Rev. B23 (1981) 2923.
[5] G.J. Galvin, M.O. Thompson, J.W. Mayer, R.B. Hammond, N. Paulter, P.S. Peercy, Phys. Rev. Lett. 48 (1982) 33.
[6] S.R. Stiffler, M.O. Thompson, P.S. Peercy, Phys. Rev. Lett. 60 (1988) 2519.
[7] T. Sameshima, M. Hara, S. Usui, Jpn. J. Appl. Phys. 28 (1989) 2131.
[8] R.S. Sussmann, A.J. Harris, R. Ogden, J. Noncrystalline Solid 35–36 (1980) 249.
[9] T. Sameshima, S. Usui, M. Sekiya, IEEE Electron Device Lett. 7 (1986) 276.
[10] E. Fogarassy, B. Prevot, S. De Unamuno, E. Elliq, H. Pattyn, E.L. Mathe, A. Naudon, Appl. Phys. A 56 (1993) 365.
[11] K.F. Lee, T.J. Stultz, J.F. Gibbons, in: J.F. Gibbons (Ed.), Beam Recrystallized Polycrystalline Silicon Properties, vol. 17, Academic Press, Inc., 1984, p. 289.
[12] N.M. Hawkins, J.G. Black, C.N. Griffiths, Appl. Phys. Lett. 40 (1982) 319.
[13] J.C. Sturm, J.F. Gibbons, IEEE Trans. Electron Device Lett. EDL-3 (1982) 369.
[14] T. Sameshima, N. Andoh, Jpn. J. Appl. Phys. 44 (2005) 7305.
[15] N. Sano, M. Maki, N. Andoh, T. Sameshima, Jpn. J. Appl. Phys. 46 (2007) 1254.
[16] M. Sekiya, M. Hara, N. Sano, T. Sameshima, IEEE Electron Device Lett. 15 (1996) 69.
[17] J.S. Im, H.J. Kim, Appl. Phys. Lett. 63 (1993) 1969.
[18] O.H. Chang-Ho, M. Ozawa, M. Matsumura, Jpn. J. Appl. Phys. 37 (1998) L492.
[19] Paul Ch. van der Wilt, B.D. van Dijk, G.J. Bertens, R. Ishihara, C.I.M. Beenakker, Appl. Phys. Lett. 79 (2001) 1819.
[20] M. Nakata, H. Okumura, H. Kanoh, H. Hayama, Proc. in Asia Display/IMID'04 (Tegu), 2004, p. 412.
[21] C.H. Kim, I.H. Song, W.J. Nam, M.K. Han, IEEE Electron Device Lett. 23 (2002) 315.
[22] A. Hara, F. Takeuchi, M. Takei, K. Suga, K. Yoshino, M. Chida, Y. Sano, N. Sasai, Jpn. J. Appl. Phys. 37 (2002) L5.
[23] M. Tai, M. Hatano, S. Yamaguchi, T. Noda, P. S-Kee, T. Shiba, M. Ohkura, IEEE Trans. Electron Devices 51 (2004) 934.
[24] T. Serikawa, F. Omata, Jpn. J. Appl. Phys. 39 (2000) L393.
[25] S. Uchikoga, N. Ibaraki, Thin Solid Films 383 (2001) 19.
[26] Y. Kuo, Thin Film Transistors, Kluwer Academic Publishers, New York, 2003 (Chapters 10–13).
[27] E.I. Shtyrkov, I.B. Khaibullin, M.M. Zaripov, M.F. Galyatudinov, R.M. Bayasitov, Sov. Phys. Semicond. (Enbl. Transl.) 9 (1975) 1309.
[28] R.F. Wood, C.E. Giles, Rhys. Rev. B23 (1981) 5555.
[29] K. Ukawa, Y. Kanda, T. Sameshima, N. Sano, M. Naito, N. Hamamoto, Jpn. J. Appl. Phys. 49 (2010) 076503.

[30] T.F. Deutsch, J.C.C. Fan, C.W. Turner, R.L. Chapman, D.J. Ehrlich, R.M. Osgood Jr., Appl. Phys. Lett. 38 (1981) 144.
[31] T. Sameshima, S. Usui, M. Sekiya, J. Appl. Phys. 62 (1987) 71.
[32] T. Sameshima, H. Tomita, S. Usui, Jpn. J. Appl. Phys. 27 (1988) 1935.
[33] T. Akane, T. Nii, S. Matumoto, Jpn. J. Appl. Phys. 31 (1992) 4437.
[34] M. Ametowobla, A. Esturo-Bretoín, J.R. Kohler, J.H. Werner, Proc. 31st IEEE Photovoltaic Specialists Conf., 2005, p. 1277.
[35] B.S. Tjahjono, J.H. Guo, Z. Hameiri, L. Mai, A. Sugianto, S. Wang, S.R. Wenham, Proc. 22nd European Photovoltaic Solar Energy Conf., 2007, p. 966.
[36] A. Ogane, K. Hirata, Y. Takahashi, K. Horiuchi, Y. Nishihara, Y. Takahashi, A. Kitiyanan, T. Fuyuki, Jpn. J. Appl. Phys. 48 (2009) 071201.
[37] G.S. Kousik, Z.G. Ling, P.K. Ajmera, J. Appl. Phys. 72 (1992) 141.
[38] J.M. Borrego, R.J. Gutmann, N. Jensen, O. Paz, Solid-State Electron 30 (1987) 195.
[39] G.W. 't Hooft, C. Van Opdorp, H. Veenvliet, A.T. Vink, J. Cryst. Growth 55 (1981) 173.
[40] H. Daio, F. Shimura, Jpn. J. Appl. Phys. 32 (1993) L1792.
[41] J. Sritharathikhun, C. Banerjee, M. Otsubo, T. Sugiura, H. Yamamoto, T. Satoi, A. Limmanee, A. Yamada, M. Konagai, Jpn. J. Appl. Phys. 46 (2007) 53296.
[42] Y. Takahashi, J. Nigo, A. Ogane, Y. Uraoka, T. Fuyuki, Jpn. J. Appl. Phys. 47 (2008) 5320.
[43] M. Boulou, D. Bois, J. Appl. Phys. 48 (1977) 4713.
[44] Y. Ogita, J. Appl. Phys. 79 (1996) 6954.
[45] C. Munakata, Jpn. J. Appl. Phys. 43 (2004) L1394.
[46] T. Sameshima, K. Betsuin, T. Mizuno, N. Sano, Jpn. J. Appl. Phys. 51 (2012), 03CA04-1–6.
[47] M. Hasumi, J. Takenezawa, T. Nagao, T. Sameshima, Jpn. J. Appl. Phys. 50 (2011), 03CA03-1–4.
[48] T. Sameshima, H. Hayasaka, T. Haba, Jpn. J. Appl. Phys. 48 (2009), 021204-1–7.
[49] T. Sameshima, T. Nagao, S. Yoshidomi, K. Kogure, M. Hasumi, Jpn. J. Appl. Phys. 50 (2011), 03CA02-1–6.
[50] T. Sameshima, R. Ebina, K. Betsuin, Y. Takiguchi, M. Hasumi, Jpn. J. Appl. Phys. 52 (2013), 011801-1–6.
[51] E.D. Palk, Handbook of Optical Constants of Solids, Academic Press, London, 1985, pp. 547.
[52] Y. Taur, T. Ning, Fundamental of Modern VLSI Physics, Cambridge University Press, Cambridge, U.K., 1998 (Chapter 2).
[53] A.S. Groove, Physics and Technology of Semiconductor Devices, Wiley, New York, 1967 (Chapter 5).
[54] T. Sameshima, S. Shibata, Jpn. J. Appl. Phys. 53 (2014) 061301.
[55] M. Hasumi, T. Nakamura, S. Yoshidomi, T. Sameshima, Jpn. J. Appl. Phys. 53 (2014) 05FV05.